

Prediction of novel layered indium halide superconductors

Zhi-Hong Yuan(袁志红), Jing-Jing Meng(孟静静), Rui Liu(刘瑞), Peng-Yu Zheng(郑鹏宇), and Zhi-Ping Yin(殷志平)

Citation: Chin. Phys. B, 2024, 33 (**10**): 107401. DOI: 10.1088/1674-1056/ad6a09
Journal homepage: http://cpb.iphy.ac.cn; http://iopscience.iop.org/cpb

What follows is a list of articles you may be interested in

Half-integer Shapiro steps in MgB_2 focused He ion beam Josephson junctions

Dali Yin(殷大利), Xinwei Cai(蔡欣炜), Tiequan Xu(徐铁权), Ruining Sun(孙瑞宁), Ying Han(韩颖), Yan Zhang(张焱), Yue Wang(王越), and Zizhao Gan(甘子钊)
Chin. Phys. B, 2024, 33 (**8**): 087404. DOI: 10.1088/1674-1056/ad4d62

Two-fold symmetry of the in-plane resistance in kagome superconductor $Cs(V_{1-x}Ta_x)_3Sb_5$ with enhanced superconductivity

Zhen Zhao(赵振), Ruwen Wang(王汝文), Yuhang Zhang(张宇航), Ke Zhu(祝轲), Weiqi Yu(余维琪), Yechao Han(韩烨超), Jiali Liu(刘家利), Guojing Hu(胡国静), Hui Guo(郭辉), Xiao Lin(林晓), Xiaoli Dong(董晓莉), Hui Chen(陈辉), Haitao Yang(杨海涛), and Hong-Jun Gao(高鸿钧)
Chin. Phys. B, 2024, 33 (**7**): 077406. DOI: 10.1088/1674-1056/ad4ffa

Observation of parabolic electron bands on superconductor $LaRu_2As_2$

Xingtai Zhou(周兴泰), Geng Li(李更), Lulu Pan(潘禄禄), Zichao Chen(陈子超), Meng Li(李萌), Yanhao Shi(时延昊), Haitao Yang(杨海涛), and Hong-Jun Gao(高鸿钧)
Chin. Phys. B, 2024, 33 (**7**): 077401. DOI: 10.1088/1674-1056/ad4d63

Revisit of the anisotropic vortex states of 2H-$NbSe_2$ towards the zero-field limit

Fan Zhang(张凡), Xingyuan Hou(侯兴元), Yuxuan Jiang(姜宇轩), Zongyuan Zhang(张宗源), Yubing Tu(涂玉兵), Xiangde Zhu(朱相德), Genfu Chen(陈根富), and Lei Shan(单磊)
Chin. Phys. B, 2024, 33 (**6**): 067401. DOI: 10.1088/1674-1056/ad362d

Nonreciprocal transport in the superconducting state of the chiral crystal $NbGe_2$

Yonglai Liu(刘永来), Xitong Xu(许锡童), Miao He(何苗), Haitian Zhao(赵海天), Qingqi Zeng(曾庆祺), Xingyu Yang(杨星宇), Youming Zou(邹优鸣), Haifeng Du(杜海峰), and Zhe Qu(屈哲)
Chin. Phys. B, 2024, 33 (**5**): 057402. DOI: 10.1088/1674-1056/ad334b

---

Prediction of novel layered indium halide superconductors

Zhi-Hong Yuan(袁志红)[1,2], Jing-Jing Meng(孟静静)[1], Rui Liu(刘瑞)[1], Peng-Yu Zheng(郑鹏宇)[1], and Zhi-Ping Yin(殷志平)[1,3,†]

[1] *School of Physics & Astronomy and Center for Advanced Quantum Studies, Beijing Normal University, Beijing* 100875, *China*
[2] *School of Physics and Information Engineering, Shanxi Normal University, Taiyuan* 030031, *China*
[3] *Key Laboratory of Multiscale Spin Physics (Ministry of Education), Beijing Normal University, Beijing* 100875, *China*

(Received 6 May 2024; revised manuscript received 20 July 2024; accepted manuscript online 1 August 2024)

We design two new layered indium halide compounds $LaOInF_2$ and $LaOInCl_2$ by means of first-principles calculations and evolutionary crystal structure prediction. We find both compounds crystallize in a tetragonal structure with $P4/nmm$ space group and have indirect band gaps of 2.58 eV and 3.21 eV, respectively. By substituting O with F, both of them become metallic and superconducting at low temperature. The F-doping leads to strong electron–phonon coupling in the low-energy acoustic phonon modes which is mainly responsible for the induced superconductivity. The total electron–phonon coupling strength are 1.86 and 1.48, while the superconducting transition temperature (T_c) are about 7.2 K and 6.5 K with 10% and 5% F doping for $LaOInF_2$ and $LaOInCl_2$, respectively.

Keywords: superconductor, $LaOInF_2$, $LaOInCl_2$, electron–phonon coupling

PACS: 74.10.+v, 74.70.–b, 63.20.dk, 63.20.kd **DOI:** 10.1088/1674-1056/ad6a09

1. Introduction

Superconducting materials have attracted significant attention worldwide due to their promising applications. The search for new high-temperature superconductors has long been an important subject of both theoretical and experimental studies. With the rapid advancements in computational science and algorithms, computational simulation has become a crucial pathway in the exploration of new superconductors, which offers valuable insights that help guide experimental design and material optimization.[1–4]

Layered materials have attracted increasing interests in superconducting research due to their rich structural variation, in which the superconductivity can be induced and improved through doping, substitution, intercalation, and applying pressure.[5] There are a number of superconductors possessing layered structures, such as the MgB_2,[6] Sr_2RuO_4,[7] (Hf,Zr)NCl,[8] and Cu-based,[9] Fe-based,[10] Bi-based,[11] Ni-based[12] superconductors. However, the superconducting mechanism of most layered superconductors is still elusive,[10,12–14] it is important to discover new layered superconductors to accelerate the understanding of superconductivity. Recently, we predicted two new layered compounds $LaOTlF_2$ and $LaOTlCl_2$ by means of first-principle calculations.[15] Both of them crystallize in a layered tetragonal structure with $P4/nmm$ space group. Similar to BiS_2-based superconductors, their parent phases are insulators, and superconductivity was introduced by partially substituting O with F. The T_c are predicted to reach about 8.6 K and 8.1 K in optimally doped $La(O,F)TlF_2$ and $La(O,F)TlCl_2$ compounds.[15]

Considering that thallium (Tl) is a toxic metal element, so it is dangerous to synthesize compounds containing Tl. We further studied layered indium (In) halide-based compounds, which do not have toxic elements, thus can be synthesized safely in the laboratory. Previously, a bulk indium halide-based compound $CsInF_3$[16] was predicted to have a superconducting temperature T_c about 24 K with sufficient hole doping and pressure, which is similar to $CsTlF_3$.[17] However, hole-doping these bulk materials is very difficult, which has been unsuccessful yet. To overcome the difficulties of doping in bulk materials, we aim to design layered indium halide-based compounds. Our results demonstrate that F-doped layered $LaOInF_2$ and $LaOInCl_2$ compounds are candidates for superconductors.

2. Computational details

We find that there is no information on the $LaOInF_2$ and $LaOInCl_2$ compounds in the ICSD (Inorganic Crystal Structure Database),[18] thus the widely used crystal structure prediction software CALYPSO (Crystal structure AnaLYsis by Particle Swarm Optimization)[19] and USPEX (Universal Structure Predictor: Evolutionary Xtallography)[20] are employed to find the ground state crystal structures of $LaOInF_2$ and $LaOInCl_2$. To simulate the electron-doping systems, we replace O with F by the virtual crystal approximation (VCA) method.[21–24]

The structural, electronic, and lattice-dynamical properties are obtained based on the density functional theory (DFT) and density functional perturbation theory (DFPT)[25] using the Quantum ESPRESSO code.[26] We adopt the norm-conserving pseudopotential[27] to describe the interactions between electrons and ion cores. The Perdew–Burke–Ernzerhof (PBE)[28] is used for the exchange–correlation functional,

†Corresponding author. E-mail: yinzhiping@bnu.edu.cn

© 2024 Chinese Physical Society and IOP Publishing Ltd

where the In $4d^{10}5s^25p^1$, La $5s^25p^65d^16s^2$, F $2s^22p^5$, Cl $3s^23p^5$, and O $2s^22p^4$ orbitals are included as valence electrons. The kinetic energy cut-off and the charge density cut-off of the plane wave basis are set to be 100 Ry (1 Ry = 13.6056923(12) eV) and 400 Ry, respectively. For each doping case, the lattice constants and atomic positions are fully relaxed by minimizing the total energy. In calculations, the Brillouin zone integration is performed with a Monkhorst–Pack grid of 16×16×4 k-points. The dynamical matrices and phonon perturbation potentials are calculated within the framework of DFPT[25] on a Γ-centered 8×8×2 q mesh. In addition, considering the DFT-PBE typically underestimates the band gaps of insulators, we use the strongly-constrained and appropriately-normed (SCAN) functional [29] to estimate the band gaps of the parent compounds.

The electron–phonon coupling (EPC) simulations are implemented in the EPW (Electron–phonon Wannier) package.[30,31] Six maximally localized Wannier functions (three p states for each In atoms) are used to describe the electronic structure near the Fermi level. We take the 16×16×2 k-mesh and 8×8×2 q-mesh as coarse grids and then interpolate to the 64×64×16 k-mesh and 32×32×8 q-mesh dense grids, respectively. The Dirac δ-functions for electrons and phonons are replaced by smearing functions with widths of 20 meV and 0.2 meV, respectively.

3. Results and discussion

3.1. Stability and structures of $LaOInF_2$ and $LaOInCl_2$

Figure 1 shows the predicted crystal structures of two compounds. Both of them have a tetragonal structure with the space group of $P4/nmm$ (No. 129), in which double InF_2/$InCl_2$ layers and LaO layers alternately stacked along the c axis, forming the layered structure. Each unit cell has two formula units with ten atoms. A notable difference of the two compounds is the atom positions of halogen ions: In $LaOInF_2$, all the F ions occupy only one type of Wyckoff positions $4f$, whereas in $LaOInCl_2$, there are two distinct sites for the Cl ions (Cl-1 and Cl-2), of which Cl-1 ions and Cl-2 ions are very close to the In and La ions, respectively.

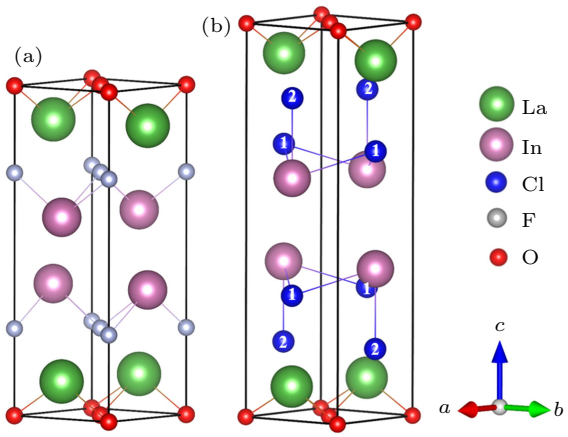


Fig. 1. Crystal structures of (a) $LaOInF_2$ and (b) $LaOInCl_2$. The numbers 1 and 2 in the blue balls of panel (b) represent the two inequivalent sites of Cl atoms. The figures are generated by the software VESTA.[32]

The detailed lattice parameters and Wyckoff atomic coordinates are summarized in Table 1.

To verify whether these two compounds are stable with the tetragonal structure, a double check was carried out on energetic stability and dynamic stability. To check the energetic stability, two possible reactions are considered to synthesize $LaOInF_2$ and $LaOInCl_2$ compounds respectively.

$$3\mathrm{LaOF} + \mathrm{InF_3} + 2\mathrm{In} \longrightarrow 3\mathrm{LaOInF_2} + Q,$$
$$\mathrm{LaCl} + \mathrm{InOCl} \longrightarrow \mathrm{LaOInCl_2} + Q,$$

where Q is the emitted energy during the reaction. By using the structures of the related reactants taken from the ICSD,[18] our calculations suggest the two reactions release about 2.59 eV (249 kJ/mol) and 3.95 eV (381 kJ/mol) energy per $LaOInF_2$ unit and per $LaOInCl_2$ unit, respectively. The results confirm that the above reactions are energetically favored.

To further examine the dynamic stability of the two compounds, their phonon dispersion curves are calculated using DFPT and the results are depicted in Figs. 2(a) and 3(a). The absence of imaginary frequency modes indicates the dynamic stability of $LaOInF_2$ and $LaOInCl_2$ compounds. The satisfactory energetic stability and dynamic stability indicates that these two compounds are promising to be synthesized in future experiments from the theoretical point of view.

Table 1. The calculated lattice parameters and Wyckoff positions of $LaOInF_2$ and $LaOInCl_2$.

	$LaOInF_2$				$LaOInCl_2$			
a (Å)	4.135				4.211			
c (Å)	11.185				13.997			
	Wyckoff positions			site	Wyckoff positions			site
La	0.0000	0.5000	0.1132	2c	0.0000	0.5000	0.0866	2c
O	0.0000	0.0000	0.0000	2a	0.0000	0.0000	0.0000	2a
In	0.5000	0.0000	0.3890	2c	0.5000	0.0000	0.3840	2c
F/Cl	0.0000	0.0000	0.2638 (F)	4f	0.0000	0.5000	0.3174 (Cl-1)	2c
					0.5000	0.0000	0.1805 (Cl-2)	2c

Moreover, the total and partial phonon density of states (DOS) are also calculated and shown in Figs. 2(b) and 3(b). For both compounds, the low-frequency phonons are mainly from the vibrations of In atoms, while the high-frequency modes are mostly related to the vibrations of O atoms. The intermediate-frequency region about 90 cm^{-1}–215 cm^{-1} for $LaOInF_2$ and about 80 cm^{-1}–225 cm^{-1} for $LaOInCl_2$ involves the vibrations of La and F/Cl atoms (F for $LaOInF_2$ and Cl for $LaOInCl_2$). In addition, the frequency modes between 215 cm^{-1} and 315 cm^{-1} mostly correspond to the vibrations of F atoms for $LaOInF_2$. However, in the case of $LaOInCl_2$, since there is a greater mass difference between Cl and O than that between F and O, a wider optical phonon gap was observed in the range of 225 cm^{-1}–325 cm^{-1}.

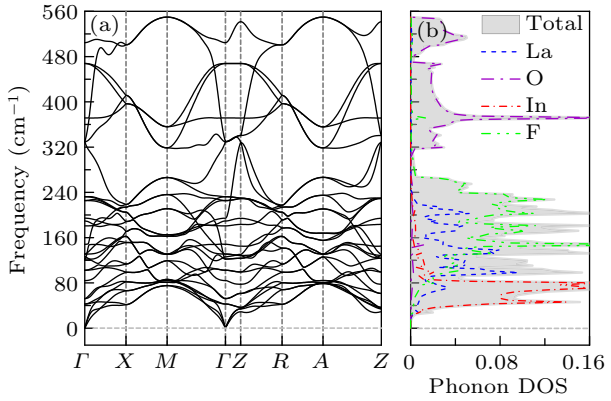


Fig. 2. Phonon dispersion curves and phonon density of states (DOS) of $LaOInF_2$.

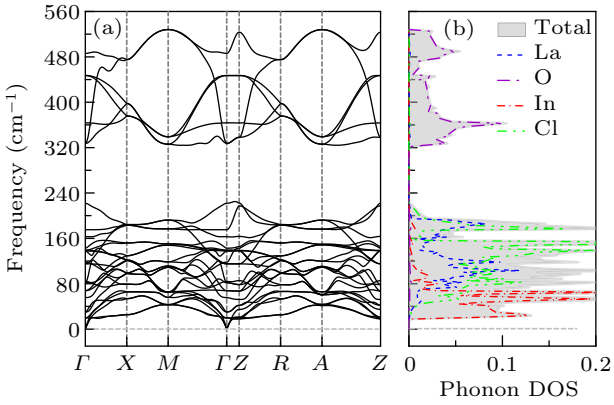


Fig. 3. Phonon dispersion curves and phonon density of states of $LaOInCl_2$.

3.2. Electronic structures of $LaOInF_2$ and $LaOInCl_2$

With the reliable crystal structure, we next explored the electronic structures of $LaOInF_2$ and $LaOInCl_2$ using the SCAN functional. The calculated electronic band structures and density of states (DOS) in the energy range of [−3.0 eV, 5.5 eV] are shown in Figs. 4 and 5, which indicates both compounds are insulators with indirect band gaps of 2.58 eV and 3.21 eV for $LaOInF_2$ and $LaOInCl_2$, respectively. One major difference is that the valence band maximum and conduction band minimum of the two compounds are at different k points. The partial density of states in Figs. 4(b) and 5(b) show that the bottom of conduction bands for both compounds are mainly from In-5p orbitals, while the contribution from La-5d orbitals are mainly located above 4.8 eV/5.0 eV (4.8 eV for $LaOInF_2$ and 5.0 eV for $LaOInCl_2$). For the valence bands, both In-5s and F-2p/Cl-3p orbitals have significant contribution to the DOS near the Fermi level (0.0 eV). The lower part of valence bands from −3.0 eV to −0.33 eV for $LaOInF_2$ and from −3 eV to −0.46 eV for $LaOInCl_2$ mainly originates from the O-2p, La-5d, and F-2p/Cl-3p orbitals.

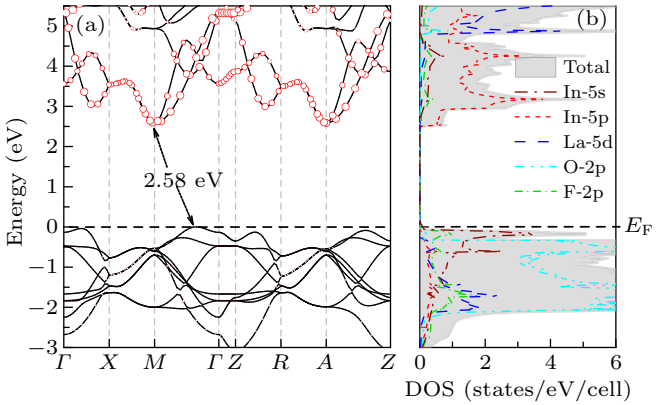


Fig. 4. (a) Electronic band structure and (b) density of state (DOS) of $LaOInF_2$. The red circles in panel (a) are used to denote the In-5p orbital character in different bands where the radius of the circle is proportional to the orbital weight. The black horizontal dash line represents the Fermi energy level.

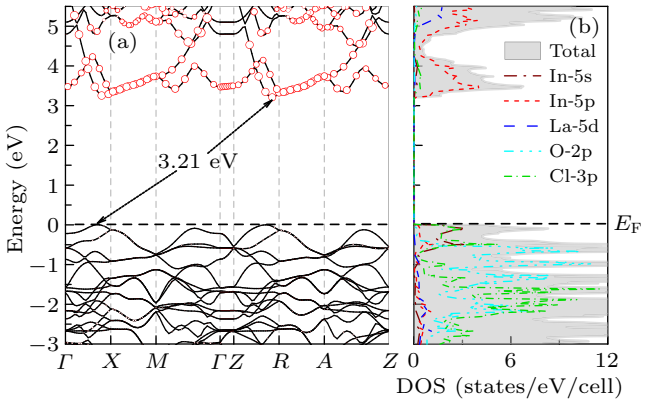


Fig. 5. (a) Electronic band structure and (b) density of state of $LaOInCl_2$. The red circles in panel (a) are used to denote the In-5p orbital character in different bands where the radius of the circle is proportional to the orbital weight. The black horizontal dash line represents the Fermi energy level.

3.3. Electronic properties of F-doped $LaOInF_2$ and $LaOInCl_2$

In the following section, the effects of electron-doping on $LaOInF_2$ and $LaOInCl_2$ compounds are investigated by substituting O with F, namely, forming $LaO_{1-x}F_xInF_2$ and $LaO_{1-x}F_xInCl_2$ with F doping level x. The partial substitution of F^- for O^{2-} is implemented by the VCA method. The fully relaxed lattice constants of each doping level are displayed in Table 2. The increasing doping level leads to a monotonous reduction of the lattice parameters a and c, due to the fact that the radius of F atom is slightly smaller than that of O atom.

Table 2. The lattice constants of different F doping level (x) on the parent compounds $LaOInF_2$ and $LaOInCl_2$.

	$LaO_{1-x}F_xInF_2$				$LaO_{1-x}F_xInCl_2$	
x	0	0.05	0.1	0.15	0	0.05
a (Å)	4.135	4.128	4.122	4.117	4.211	4.208
c (Å)	11.185	10.991	10.898	10.849	13.997	13.895

The calculated electronic band structures and DOS as well as the Fermi surface (FS) of $LaO_{0.9}F_{0.1}InF_2$ and $LaO_{0.95}F_{0.05}InCl_2$ are displayed in Figs. 6 and 7. For $LaO_{0.9}F_{0.1}InF_2$, the conduction bands around the M (A) point cross the Fermi energy, which results in two overlapped cylindroids electron-like FS around M (A) point (Fig. 6(c)). In case of $LaO_{0.95}F_{0.05}InCl_2$, the conduction bands around the X (R) point cross the Fermi energy, which results in two separated irregularly cylindrical barrel electron-like FS near X (R) point (Fig. 7(c)). For two compounds, the DOS near the Fermi energy are mainly from the In-5p states (Figs. 6(b) and 7(b)). $LaO_{0.95}F_{0.05}InCl_2$ has higher $N(E_F)$ (electronic DOS at the Fermi energy) than that of $LaO_{0.9}F_{0.1}InF_2$ (and $LaO_{0.95}F_{0.05}InF_2$). The results of $N(E_F)$ are listed in Table 3, the larger $N(E_F)$ of $LaO_{0.95}F_{0.05}InCl_2$ may lead to a higher T_c.

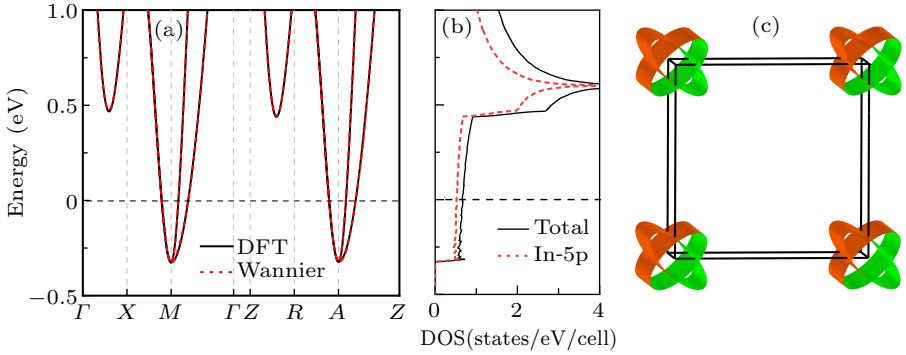


Fig. 6. (a) Electronic band structure, (b) electronic density of states, and (c) corresponding Fermi surface of $LaO_{0.9}F_{0.1}InF_2$. In panel (a), the black lines are calculated by DFT, while the red dotted line is obtained through maximally localized Wannier functions interpolation.

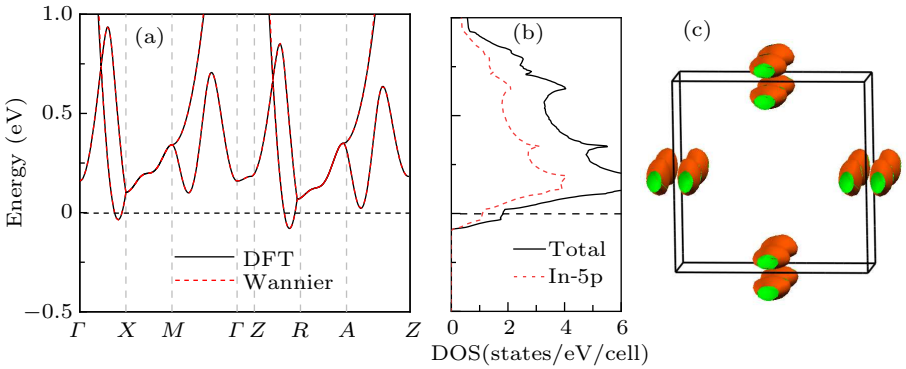


Fig. 7. (a) Electronic band structure, (b) electronic density of states, and (c) corresponding Fermi surface of $LaO_{0.95}F_{0.05}InCl_2$. In panel (a), the black lines are calculated by DFT, while the red dotted line is obtained through maximally localized Wannier functions interpolation.

3.4. Electron–phonon coupling of F-doped compounds

We now discuss the lattice dynamical properties and estimate the electron–phonon coupling of $LaO_{0.9}F_{0.1}InF_2$ and $LaO_{0.95}F_{0.05}InCl_2$. Reliable EPC results require very dense sampling of both phonon and electron momentum, so the Wannier interpolation technique are used, which can maintain a reasonable computational cost while making the EPC quantities convergent. Figures 6(a) and 7(a) reveal the Wannier interpolated band structures are in good agreement with those obtained by first-principles calculations, which forms a solid foundation for our EPW calculations. The calculated phonon dispersion curves (the size of red dots superimposed on the phonon dispersion curves is proportional to EPC coefficient λ_{qv}) and the Eliashberg phonon spectral function $\alpha^2F(\omega)$ as well as the cumulative frequency dependence of electron–phonon coupling $\lambda(\omega)$ of $LaO_{0.9}F_{0.1}InF_2$ and $LaO_{0.95}F_{0.05}InCl_2$ are shown in Figs. 8 and 9. The absence of any imaginary frequency confirms their dynamical stability.

For $LaO_{0.9}F_{0.1}InF_2$, significant phonon softening can be seen in the lowest phonon branches along the Γ–X (Z–R) and Γ–M (Z–A) directions. The large softening of acoustic modes are associated with large contributions to EPC, which is also supported by the $\alpha^2F(\omega)$ shown in Fig. 8(b). The $\lambda(\omega)$ indicates these softening modes contribute about $\sim 70\%$ of the total EPC strength. This phenomenon suggests that strong EPC at higher F doping levels may lead to lattice instability. Indeed, our calculations show that when F doping level is more than 0.1 ($x > 0.1$), the frequencies of the lowest phonon mode become imaginary around $\boldsymbol{q} = (0, 0.125, 0)/(0, 0.125, 0.5)$, and $\boldsymbol{q} = (0.125, 0.125, 0)/(0.125, 0.125, 0.5)$ (The $\boldsymbol{q}$ points

are given in the units of the three reciprocal lattice vectors of the primitive unit cell). For the $LaO_{0.95}F_{0.05}InCl_2$, figure 9(b) reveals that low frequency vibration modes around $\boldsymbol{q} = (0,0.165,0)/(0,0.165,0.5)$, and $\boldsymbol{q} = (0.125,0.125,0)/(0.125,0.125,0.5)$ have large contributions to EPC. Our calculations suggest that when F doping level is more than 0.05, the lowest phonon frequencies at these $\boldsymbol{q}$ points become imaginary. The $\alpha^2F(\omega)$ and $\lambda(\omega)$ curves exhibit that low-frequency vibrational modes (< 56 cm^{-1}) which mainly corresponding to the vibrations of the acoustic branches involving mainly the In atoms contribute about 74% of total λ for $LaO_{0.95}F_{0.05}InCl_2$. Meanwhile, we find the $\lambda(\omega)$ curves increases gently in the middle-frequency region about 56 cm^{-1} to 225 cm^{-1}. It can be seen that the strong EPC is the driving force for both the phonon softening and superconductivity of $LaO_{0.9}F_{0.1}InF_2$ and $LaO_{0.95}F_{0.05}InCl_2$.

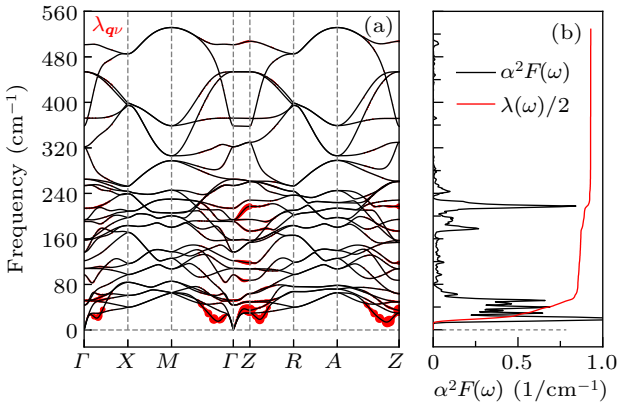


Fig. 8. (a) Phonon dispersion curves of $LaO_{0.9}F_{0.1}InF_2$. The sizes of red dots on the phonon dispersions curves correspond to the strengths of the mode EPC $\lambda_{q\nu}$. (b) Eliashberg spectral function $\alpha^2F(\omega)$ (black line) and cumulative frequency dependence of EPC $\lambda(\omega)$ (red line) of $LaO_{0.9}F_{0.1}InF_2$. The results of $\alpha^2F(\omega)$ are integrated on a homogeneous fine k-point grid containing 64×64×16 points, and a fine homogeneous q-mesh with 32×32×8 points.

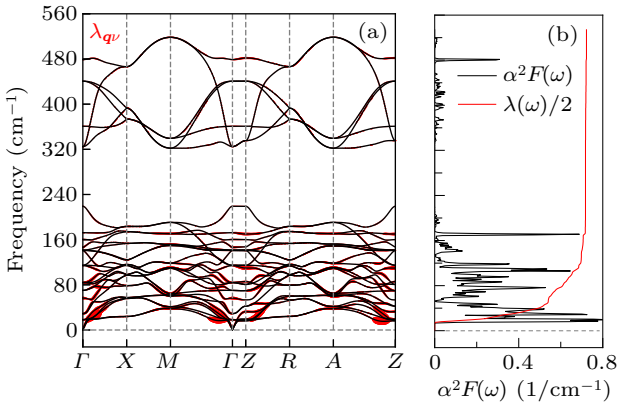


Fig. 9. (a) Phonon dispersions curves of $LaO_{0.95}F_{0.05}InCl_2$. The sizes of red dots on the phonon dispersions curves correspond to the strengths of the mode EPC $\lambda_{q\nu}$. (b) Eliashberg spectral function $\alpha^2F(\omega)$ (black line) and cumulative frequency dependence of EPC $\lambda(\omega)$ (red line) of $LaO_{0.95}F_{0.05}InCl_2$. The results of $\alpha^2F(\omega)$ are integrated on a homogeneous fine k-point grid containing 64×64×16 points, and a fine homogeneous q-mesh with 32×32×8 points.

In addition, the analysis of atomic vibrational modes of low-frequency phonons shows that the vibrations of In atoms contribute significantly to the EPC for $LaO_{0.9}F_{0.1}InF_2$ and $LaO_{0.95}F_{0.05}InCl_2$. For example, for $LaO_{0.9}F_{0.1}InF_2$, the phonon mode with frequency about 34.6 cm^{-1} at Z point mainly corresponds to the out-of-plane vibrations of In atoms moving out-of-phase between two InF_2 layers (Fig. 10(a)); the phonon mode with frequency about 17.8 cm^{-1} at $\boldsymbol{q} = (0.15,0.15,0)$ is also primarily the vibrations of In atoms moving out-of-phase between two InF_2 layers (Fig. 10(b)). For $LaO_{0.95}F_{0.05}InCl_2$, the phonon modes with frequency about 15.8 cm^{-1} at $\boldsymbol{q} = (0.125,0.125,0.5)$ and 16.5 cm^{-1} at $\boldsymbol{q} = (0.1,0.1,0.0)$ are primarily from the in-plane vibrations of In atoms moving out-of-phase between two $InCl_2$ layers (Fig. 10(c)).

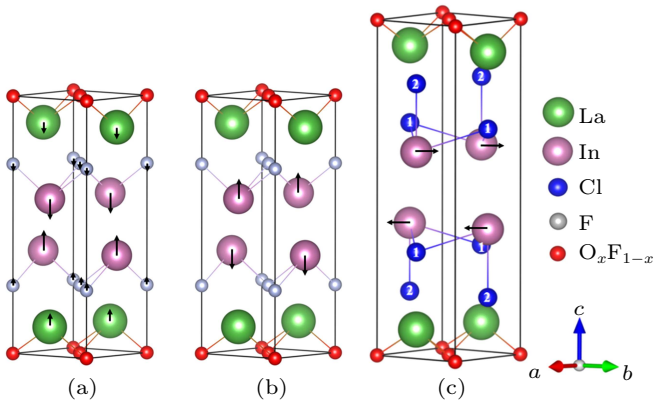


Fig. 10. Three important vibrational modes with large electron–phonon coupling. (a) The phonon mode at Z with frequency $\omega \sim 34.6$ cm^{-1} for $LaO_{0.9}F_{0.1}InF_2$, (b) The phonon mode at $\boldsymbol{q} = (0.15,0.15,0)$ with frequency $\omega \sim 17.8$ cm^{-1} for $LaO_{0.95}F_{0.05}InF_2$, (c) The phonon modes at $\boldsymbol{q} = (0.125,0.125,0.5)$ with frequency $\omega \sim 15.8$ cm^{-1} and at $\boldsymbol{q} = (0.1,0.1,0.0)$ with frequency $\omega \sim 16.5$ cm^{-1} for $LaO_{0.95}F_{0.05}InCl_2$.

By integrating $\alpha^2F(\omega)$, the total EPC constant λ and the logarithmic average phonon frequency $\omega_{\log}$ are obtained, which are listed in Table 3. The decrease in $\omega_{\log}$ with increased F-doping level is the consequence of the phonon softening behavior discussed above. Considering the strong EPC of these doped-compounds, the T_c are estimated through the revised Allen–Dynes formula with $\mu^* = 0.1$,[33] and the resulting T_c (K) values are also listed in Table 3. It can be seen that the λ of $LaO_{0.9}F_{0.1}InF_2$ is significantly larger than that of $LaO_{0.95}F_{0.05}InF_2$, which is due to the severe phonon softening of $LaO_{0.9}F_{0.1}InF_2$. In addition, the λ of $LaO_{0.95}F_{0.05}InCl_2$ is larger than that of $LaO_{0.95}F_{0.05}InF_2$, which is attributed to the higher $N(E_F)$ of $LaO_{0.95}F_{0.05}InCl_2$.

Table 3. Calculated electronic density of states at Fermi level $N(E_F)$ (states/spin/eV/cell), logarithmic average phonon frequency $\omega_{\log}$ (K), total electron–phonon coupling λ, and superconducting transition temperature T_c (K) for $LaO_{0.95}F_{0.05}InF_2$ and $LaO_{0.9}F_{0.1}InF_2$ as well as $LaO_{0.95}F_{0.05}InCl_2$.

Compound	$N(E_F)$	λ	$\omega_{\log}$	T_c
$LaO_{0.95}F_{0.05}InF_2$	0.31	0.79	88.5	3.9
$LaO_{0.9}F_{0.1}InF_2$	0.33	1.86	43.3	7.2
$LaO_{0.95}F_{0.05}InCl_2$	0.87	1.48	50.5	6.5

4. Conclusions

Based on first-principle calculations and evolutionary crystal structure search, we predicted two new layered indium halide compounds $LaOInF_2$ and $LaOInCl_2$, both of them are energetically and dynamically stable with the space group of $P4/nmm$ (129). The electronic structure calculations suggest that $LaOInF_2$ and $LaOInCl_2$ are insulators with indirect band gaps of 2.58 eV and 3.21 eV, respectively, which become metallic by substituting O with F. The lattice dynamics and electron–phonon coupling calculations suggest the F-doped compounds have large EPC strength, which is mainly contributed by the low-energy acoustic phonon modes. Based on the Wannier interpolation technique, the T_c values of $LaO_{0.9}F_{0.1}InF_2$ and $LaO_{0.95}F_{0.05}InCl_2$ reached about 7.2 K and 6.5 K with λ of 1.86 and 1.48, respectively. We expect that the novel superconductors with the InF_2 or $InCl_2$ superconducting layer will open a new field in physics and chemistry of layered superconductors.

Acknowledgements

Project supported by the Fundamental Research Funds for the Central Universities (Grant No. 2243300003), the National Natural Science Foundation of China (Grant No. 12074041), and the Fundamental Research Program of Shanxi Province, China (Grant No. 202203021222228). The calculations were carried out with high performance computing cluster of Beijing Normal University in Zhuhai.

References

[1] Errea I, Calandra M, Pickard C J, Nelson J, Needs R J, Li Y, Liu H, Zhang Y, Ma Y and Mauri F 2015 *Phys. Rev. Lett.* **114** 157004
[2] Shi L T, Si J G, Turnbull R, Liang A, Liu P F and Wang B T 2024 *Phys. Rev. B* **109** 054512
[3] Duan Q, Zhan L, Shen J, Zhong X and Lu C 2024 *Phys. Rev. B* **109** 054505
[4] Tran H and Vu T N 2023 *Phys. Rev. Mater.* **7** 054805
[5] Mizuguchi Y 2016 *Chem. Rec.* **16** 633
[6] Nagamatsu J, Nakagawa N, Muranaka T, Zenitani Y and Akimitsu J 2001 *Nature* **410** 63
[7] Liu Y and Mao Z Q 2015 *Physica C* **514** 339
[8] Kasahara Y, Kuroki K, Yamanaka S and Taguchi Y 2015 *Physica C* **514** 354
[9] Bednorz J G and Müller K A 1986 *Z. Physik B: Condens. Matter* **64** 189
[10] Jiang H, Sun Y L, Xu Z A and Cao G H 2013 *Chin. Phys. B* **22** 087410
[11] Hoshi K and Mizuguchi Y 2021 *J. Phys.: Condens. Matter* **33** 473001
[12] Gu Q and Wen H H 2022 *The Innovation* **3** 100202
[13] Huang Y N, Ye Z F, Liu D Y and Qiu H Q 2023 *Chin. Phys. Lett.* **40** 097405
[14] Li D, Liu Y, Lu Z Y W, Li P L, Zhang Y H, Ma S, Liu J L, Lu J H, Zhang H, Liu G T, Zhou F, Dong X L and Zhao Z X 2022 *Chin. Phys. Lett.* **39** 127402
[15] Yuan Z H, Meng J J, Liu R, Zheng P Y, Ma X B, Wang G W, Yu T Y, Peng Y R and Yin Z P 2022 *Phys. Chem. Chem. Phys.* **24** 7331
[16] Kang C J and Kotliar G 2019 *Phys. Rev. Mater.* **3** 015001
[17] Yin Z P and Kotliar G 2013 *Europhys. Lett.* **101** 27002
[18] www.fiz-karlsruhe.de/icsd.html
[19] Wang Y, Lv J, Zhu L and Ma Y 2012 *Comput. Phys. Commun.* **183** 2063
[20] Glass C W, Oganov A R and Hansen N 2006 *Comput. Phys. Commun.* **175** 713
[21] Huo Z, Duan D, Ma T, Zhang Z, Jiang Q, An D, Song H, Tian F and Cui T 2023 *Matter Radiat. Extremes* **8** 038402
[22] Peng G W, Gan X P, Li Z and Zhou K C 2018 *Chin. Phys. B* **27** 086302
[23] Bellaiche L and Vanderbilt D 2000 *Phys. Rev. B* **61** 7877
[24] Liu H, Yao J, Shi J, Yang Z, Yan D, Li Y, Chen D, Feng H L, Li S, Wang Z and Shi Y 2023 *Phys. Rev. B* **108** 104504
[25] Baroni S, De Gironcoli S, Dal Corso A and Giannozzi P 2001 *Rev. Mod. Phys.* **73** 515
[26] Giannozzi P, Baroni S, Bonini N, Calandra M, Car R, Cavazzoni C, Ceresoli D, Chiarotti G L, Cococcioni M and Dabo I 2009 *J. Phys.: Condens. Matter* **21** 395502
[27] Hamann D R 2013 *Phys. Rev. B* **88** 085117
[28] Perdew J P, Burke K and Ernzerhof M 1996 *Phys. Rev. Lett.* **77** 3865
[29] Sun J, Ruzsinszky A and Perdew J P 2015 *Phys. Rev. Lett.* **115** 036402
[30] Lee H, Poncé S, Bushick K, Hajinazar S, Lafuente-Bartolome J, Leveillee J, Lian C, Lihm J M, Macheda F, Mori H, Paudyal H, Sio W H, Tiwari S, Zacharias M, Zhang X, Bonini N, Kioupakis E, Margine E R and Giustino F 2023 *npj Comput. Mater.* **9** 156
[31] Noffsinger J, Giustino F, Malone B D, Park C H, Louie S G and Cohen M L 2010 *Comput. Phys. Commun.* **181** 2140
[32] Momma K and Izumi F 2011 *J. Appl. Crystallogr.* **44** 1272
[33] Allen P B and Dynes R C 1975 *Phys. Rev. B* **12** 905